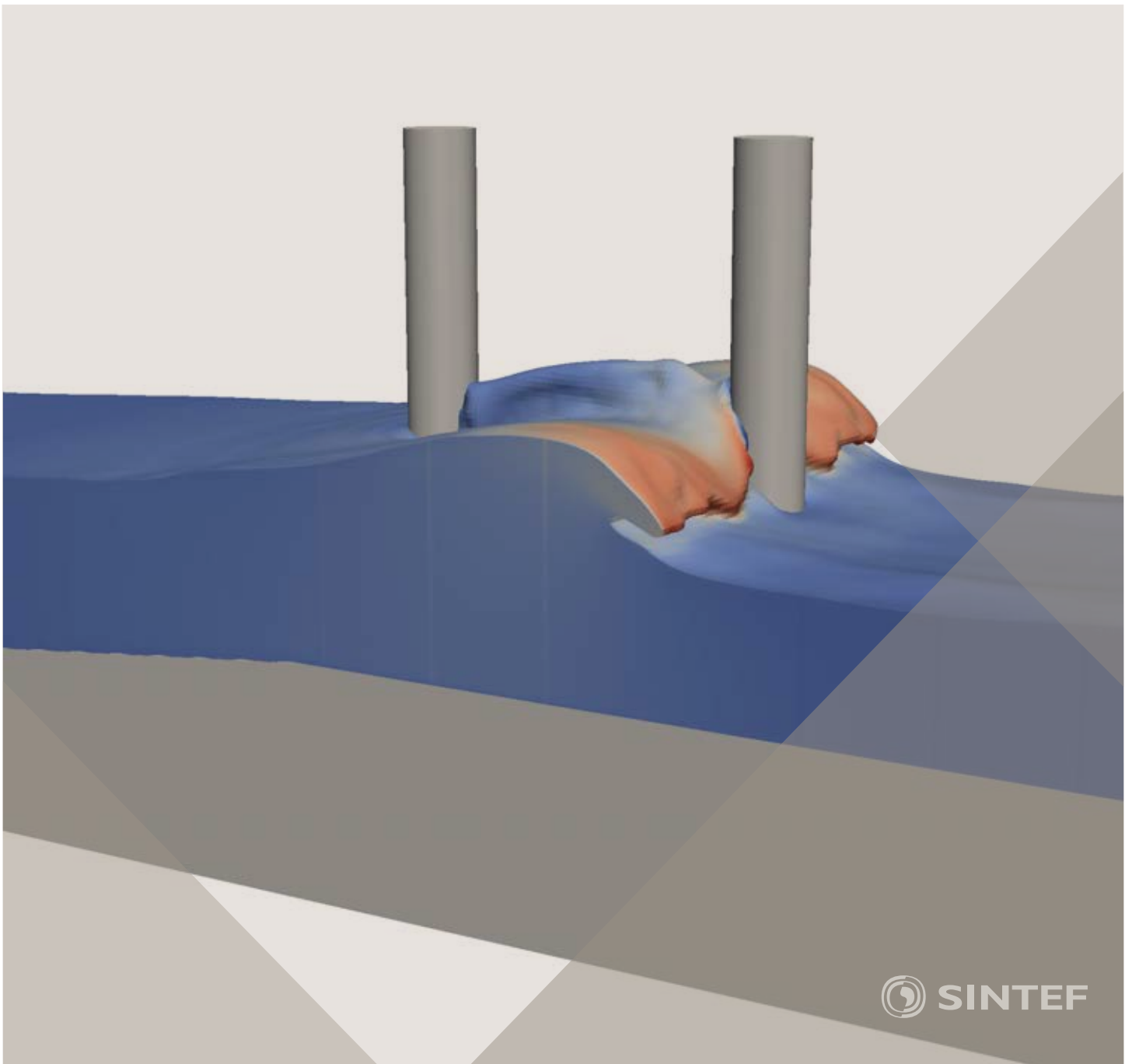


Proceedings of the 12<sup>th</sup> International Conference on  
Computational Fluid Dynamics in the Oil & Gas,  
Metallurgical and Process Industries

# Progress in Applied CFD – CFD2017



SINTEF Proceedings

Editors:

Jan Erik Olsen and Stein Tore Johansen

## **Progress in Applied CFD – CFD2017**

Proceedings of the 12<sup>th</sup> International Conference on Computational Fluid Dynamics  
in the Oil & Gas, Metallurgical and Process Industries

SINTEF Academic Press

SINTEF Proceedings no 2

Editors: Jan Erik Olsen and Stein Tore Johansen

**Progress in Applied CFD – CFD2017**

Selected papers from 10<sup>th</sup> International Conference on Computational Fluid Dynamics in the Oil & Gas, Metallurgical and Process Industries

Key words:

CFD, Flow, Modelling

Cover, illustration: Arun Kamath

ISSN 2387-4295 (online)

ISBN 978-82-536-1544-8 (pdf)

© Copyright SINTEF Academic Press 2017

The material in this publication is covered by the provisions of the Norwegian Copyright Act. Without any special agreement with SINTEF Academic Press, any copying and making available of the material is only allowed to the extent that this is permitted by law or allowed through an agreement with Kopinor, the Reproduction Rights Organisation for Norway. Any use contrary to legislation or an agreement may lead to a liability for damages and confiscation, and may be punished by fines or imprisonment

SINTEF Academic Press

Address:       Forskningsveien 3 B  
                  PO Box 124 Blindern  
                  N-0314 OSLO

Tel:             +47 73 59 30 00

Fax:            +47 22 96 55 08

[www.sintef.no/byggforsk](http://www.sintef.no/byggforsk)

[www.sintefbok.no](http://www.sintefbok.no)

**SINTEF Proceedings**

SINTEF Proceedings is a serial publication for peer-reviewed conference proceedings on a variety of scientific topics.

The processes of peer-reviewing of papers published in SINTEF Proceedings are administered by the conference organizers and proceedings editors. Detailed procedures will vary according to custom and practice in each scientific community.

## PREFACE

This book contains all manuscripts approved by the reviewers and the organizing committee of the 12th International Conference on Computational Fluid Dynamics in the Oil & Gas, Metallurgical and Process Industries. The conference was hosted by SINTEF in Trondheim in May/June 2017 and is also known as CFD2017 for short. The conference series was initiated by CSIRO and Phil Schwarz in 1997. So far the conference has been alternating between CSIRO in Melbourne and SINTEF in Trondheim. The conferences focuses on the application of CFD in the oil and gas industries, metal production, mineral processing, power generation, chemicals and other process industries. In addition pragmatic modelling concepts and bio-mechanical applications have become an important part of the conference. The papers in this book demonstrate the current progress in applied CFD.

The conference papers undergo a review process involving two experts. Only papers accepted by the reviewers are included in the proceedings. 108 contributions were presented at the conference together with six keynote presentations. A majority of these contributions are presented by their manuscript in this collection (a few were granted to present without an accompanying manuscript).

The organizing committee would like to thank everyone who has helped with review of manuscripts, all those who helped to promote the conference and all authors who have submitted scientific contributions. We are also grateful for the support from the conference sponsors: ANSYS, SFI Metal Production and NanoSim.

Stein Tore Johansen & Jan Erik Olsen



Organizing committee:

Conference chairman: Prof. Stein Tore Johansen

Conference coordinator: Dr. Jan Erik Olsen

Dr. Bernhard Müller

Dr. Sigrid Karstad Dahl

Dr. Shahriar Amini

Dr. Ernst Meese

Dr. Josip Zoric

Dr. Jannike Solsvik

Dr. Peter Witt

Scientific committee:

Stein Tore Johansen, SINTEF/NTNU

Bernhard Müller, NTNU

Phil Schwarz, CSIRO

Akio Tomiyama, Kobe University

Hans Kuipers, Eindhoven University of Technology

Jinghai Li, Chinese Academy of Science

Markus Braun, Ansys

Simon Lo, CD-adapco

Patrick Segers, Universiteit Gent

Jiyuan Tu, RMIT

Jos Derksen, University of Aberdeen

Dmitry Eskin, Schlumberger-Doll Research

Pär Jönsson, KTH

Stefan Pirker, Johannes Kepler University

Josip Zoric, SINTEF

## CONTENTS

<b>PRAGMATIC MODELLING .....</b>	<b>9</b>
On pragmatism in industrial modeling. Part III: Application to operational drilling .....	11
CFD modeling of dynamic emulsion stability .....	23
Modelling of interaction between turbines and terrain wakes using pragmatic approach .....	29
<b>FLUIDIZED BED .....</b>	<b>37</b>
Simulation of chemical looping combustion process in a double looping fluidized bed reactor with cu-based oxygen carriers.....	39
Extremely fast simulations of heat transfer in fluidized beds.....	47
Mass transfer phenomena in fluidized beds with horizontally immersed membranes .....	53
A Two-Fluid model study of hydrogen production via water gas shift in fluidized bed membrane reactors .....	63
Effect of lift force on dense gas-fluidized beds of non-spherical particles .....	71
Experimental and numerical investigation of a bubbling dense gas-solid fluidized bed .....	81
Direct numerical simulation of the effective drag in gas-liquid-solid systems .....	89
A Lagrangian-Eulerian hybrid model for the simulation of direct reduction of iron ore in fluidized beds.....	97
High temperature fluidization - influence of inter-particle forces on fluidization behavior .....	107
Verification of filtered two fluid models for reactive gas-solid flows .....	115
<b>BIOMECHANICS.....</b>	<b>123</b>
A computational framework involving CFD and data mining tools for analyzing disease in carotid artery .....	125
Investigating the numerical parameter space for a stenosed patient-specific internal carotid artery model.....	133
Velocity profiles in a 2D model of the left ventricular outflow tract, pathological case study using PIV and CFD modeling.....	139
Oscillatory flow and mass transport in a coronary artery.....	147
Patient specific numerical simulation of flow in the human upper airways for assessing the effect of nasal surgery.....	153
CFD simulations of turbulent flow in the human upper airways .....	163
<b>OIL &amp; GAS APPLICATIONS .....</b>	<b>169</b>
Estimation of flow rates and parameters in two-phase stratified and slug flow by an ensemble Kalman filter .....	171
Direct numerical simulation of proppant transport in a narrow channel for hydraulic fracturing application .....	179
Multiphase direct numerical simulations (DNS) of oil-water flows through homogeneous porous rocks .....	185
CFD erosion modelling of blind tees .....	191
Shape factors inclusion in a one-dimensional, transient two-fluid model for stratified and slug flow simulations in pipes .....	201
Gas-liquid two-phase flow behavior in terrain-inclined pipelines for wet natural gas transportation .....	207

<b>NUMERICS, METHODS &amp; CODE DEVELOPMENT .....</b>	<b>213</b>
Innovative computing for industrially-relevant multiphase flows .....	215
Development of GPU parallel multiphase flow solver for turbulent slurry flows in cyclone.....	223
Immersed boundary method for the compressible Navier–Stokes equations using high order summation-by-parts difference operators .....	233
Direct numerical simulation of coupled heat and mass transfer in fluid-solid systems .....	243
A simulation concept for generic simulation of multi-material flow, using staggered Cartesian grids.....	253
A cartesian cut-cell method, based on formal volume averaging of mass, momentum equations.....	265
SOFT: a framework for semantic interoperability of scientific software .....	273
 <b>POPULATION BALANCE .....</b>	 <b>279</b>
Combined multifluid-population balance method for polydisperse multiphase flows .....	281
A multifluid-PBE model for a slurry bubble column with bubble size dependent velocity, weight fractions and temperature.....	285
CFD simulation of the droplet size distribution of liquid-liquid emulsions in stirred tank reactors .....	295
Towards a CFD model for boiling flows: validation of QMOM predictions with TOPFLOW experiments .....	301
Numerical simulations of turbulent liquid-liquid dispersions with quadrature-based moment methods.....	309
Simulation of dispersion of immiscible fluids in a turbulent couette flow .....	317
Simulation of gas-liquid flows in separators - a Lagrangian approach.....	325
CFD modelling to predict mass transfer in pulsed sieve plate extraction columns .....	335
 <b>BREAKUP &amp; COALESCENCE .....</b>	 <b>343</b>
Experimental and numerical study on single droplet breakage in turbulent flow .....	345
Improved collision modelling for liquid metal droplets in a copper slag cleaning process .....	355
Modelling of bubble dynamics in slag during its hot stage engineering.....	365
Controlled coalescence with local front reconstruction method .....	373
 <b>BUBBLY FLOWS .....</b>	 <b>381</b>
Modelling of fluid dynamics, mass transfer and chemical reaction in bubbly flows .....	383
Stochastic DSMC model for large scale dense bubbly flows.....	391
On the surfacing mechanism of bubble plumes from subsea gas release.....	399
Bubble generated turbulence in two fluid simulation of bubbly flow .....	405
 <b>HEAT TRANSFER .....</b>	 <b>413</b>
CFD-simulation of boiling in a heated pipe including flow pattern transitions using a multi-field concept .....	415
The pear-shaped fate of an ice melting front .....	423
Flow dynamics studies for flexible operation of continuous casters (flow flex cc).....	431
An Euler-Euler model for gas-liquid flows in a coil wound heat exchanger.....	441
 <b>NON-NEWTONIAN FLOWS.....</b>	 <b>449</b>
Viscoelastic flow simulations in disordered porous media .....	451
Tire rubber extrudate swell simulation and verification with experiments .....	459
Front-tracking simulations of bubbles rising in non-Newtonian fluids.....	469
A 2D sediment bed morphodynamics model for turbulent, non-Newtonian, particle-loaded flows.....	479

<b>METALLURGICAL APPLICATIONS.....</b>	<b>491</b>
Experimental modelling of metallurgical processes .....	493
State of the art: macroscopic modelling approaches for the description of multiphysics phenomena within the electroslag remelting process .....	499
LES-VOF simulation of turbulent interfacial flow in the continuous casting mold .....	507
CFD-DEM modelling of blast furnace tapping .....	515
Multiphase flow modelling of furnace tapholes .....	521
Numerical predictions of the shape and size of the raceway zone in a blast furnace.....	531
Modelling and measurements in the aluminium industry - Where are the obstacles? .....	541
Modelling of chemical reactions in metallurgical processes.....	549
Using CFD analysis to optimise top submerged lance furnace geometries .....	555
Numerical analysis of the temperature distribution in a martensitic stainless steel strip during hardening.....	565
Validation of a rapid slag viscosity measurement by CFD.....	575
Solidification modeling with user defined function in ANSYS Fluent.....	583
Cleaning of polycyclic aromatic hydrocarbons (PAH) obtained from ferroalloys plant.....	587
Granular flow described by fictitious fluids: a suitable methodology for process simulations .....	593
A multiscale numerical approach of the dripping slag in the coke bed zone of a pilot scale Si-Mn furnace.....	599
 <b>INDUSTRIAL APPLICATIONS .....</b>	 <b>605</b>
Use of CFD as a design tool for a phosphoric acid plant cooling pond .....	607
Numerical evaluation of co-firing solid recovered fuel with petroleum coke in a cement rotary kiln: Influence of fuel moisture .....	613
Experimental and CFD investigation of fractal distributor on a novel plate and frame ion-exchanger .....	621
 <b>COMBUSTION .....</b>	 <b>631</b>
CFD modeling of a commercial-size circle-draft biomass gasifier.....	633
Numerical study of coal particle gasification up to Reynolds numbers of 1000.....	641
Modelling combustion of pulverized coal and alternative carbon materials in the blast furnace raceway .....	647
Combustion chamber scaling for energy recovery from furnace process gas: waste to value .....	657
 <b>PACKED BED.....</b>	 <b>665</b>
Comparison of particle-resolved direct numerical simulation and 1D modelling of catalytic reactions in a packed bed .....	667
Numerical investigation of particle types influence on packed bed adsorber behaviour .....	675
CFD based study of dense medium drum separation processes .....	683
A multi-domain 1D particle-reactor model for packed bed reactor applications.....	689
 <b>SPECIES TRANSPORT &amp; INTERFACES .....</b>	 <b>699</b>
Modelling and numerical simulation of surface active species transport - reaction in welding processes .....	701
Multiscale approach to fully resolved boundary layers using adaptive grids.....	709
Implementation, demonstration and validation of a user-defined wall function for direct precipitation fouling in Ansys Fluent.....	717

<b>FREE SURFACE FLOW &amp; WAVES .....</b>	<b>727</b>
Unresolved CFD-DEM in environmental engineering: submarine slope stability and other applications.....	729
Influence of the upstream cylinder and wave breaking point on the breaking wave forces on the downstream cylinder .....	735
Recent developments for the computation of the necessary submergence of pump intakes with free surfaces .....	743
Parallel multiphase flow software for solving the Navier-Stokes equations .....	752
 <b>PARTICLE METHODS .....</b>	 <b>759</b>
A numerical approach to model aggregate restructuring in shear flow using DEM in Lattice-Boltzmann simulations .....	761
Adaptive coarse-graining for large-scale DEM simulations.....	773
Novel efficient hybrid-DEM collision integration scheme.....	779
Implementing the kinetic theory of granular flows into the Lagrangian dense discrete phase model.....	785
Importance of the different fluid forces on particle dispersion in fluid phase resonance mixers .....	791
Large scale modelling of bubble formation and growth in a supersaturated liquid.....	798
 <b>FUNDAMENTAL FLUID DYNAMICS .....</b>	 <b>807</b>
Flow past a yawed cylinder of finite length using a fictitious domain method .....	809
A numerical evaluation of the effect of the electro-magnetic force on bubble flow in aluminium smelting process.....	819
A DNS study of droplet spreading and penetration on a porous medium.....	825
From linear to nonlinear: Transient growth in confined magnetohydrodynamic flows.....	831



# CFD MODELING OF A COMMERCIAL-SIZE CIRCLE-DRAFT BIOMASS GASIFIER

Hui LIU<sup>1</sup>, Robert J. CATTOLICA<sup>1\*</sup>, Reinhard SEISER<sup>1</sup>  
Chang-hsien LIAO<sup>2</sup> and Matthew SUMMERS<sup>2</sup>

<sup>1</sup>University of California, San Diego, 9500 Gilman Drive, La Jolla, CA 92093, USA

<sup>2</sup>West Biofuels, 14958 County Road 100B, Woodland, CA 95776, USA

\*Corresponding Author, E-mail: rjcat@ucsd.edu

## ABSTRACT

This work was focused on a commercial-size (2MWth.) circle-draft biomass gasifier. In this work a three-dimensional transient CFD (computational fluid dynamics) model was established to simulate the circle-draft biomass gasifier. The MP-PIC (multiphase particle-in-cell) method was applied to simulate multiphase reactive flows in the gasifier. In the MP-PIC method, the Navier-Stokes equation coupled with the large-eddy simulation (LES) was applied to describe the gas phase. The particulate phase was described in a Lagrangian way by computing the trajectories of parcels of particles solving Newtonian equations of motion for each parcel. The mass and energy transport equations were coupled with the momentum equation to simulate mass and energy transfer in the circle-draft gasifier. The heterogeneous solid-gas and homogeneous gas-phase reaction kinetics were integrated with the transport equations to simulate biomass drying, gasification, combustion, and other gas-phase reactions. The simulation results were compared with experimental data to validate the CFD model. The CFD model predicted gas species distribution, reaction zone temperatures, and producer gas composition in the circle-draft biomass gasifier.

## NOMENCLATURE

### Greek Symbols

$\alpha$	volume fraction
$\rho$	density
$\tau$	stress tensor

### Latin Symbols

$A_p$	particle surface area
$C_d$	drag model coefficient
$C_v$	specific heat capacity
$C_{p,n}$	solid species $n$ concentration
$D$	drag function
$f$	particle size distribution function
$F$	drag force
$g$	standard gravity
$k_d$	solid thermal conductivity
$m_p$	particle mass

$M_{w,p,n}$	molecular weight of solid species $n$
$Nu$	Nusselt number
$u$	velocity
$p$	pressure
$P_s$	model constant
$T$	temperature
$V$	computational cell volume

### Subscripts

$cp$	close pack condition
$g$	gas phase
$n$	solid species
$lam$	laminar flows
$t$	turbulence

## INTRODUCTION

Fossil fuels are still the primary energy sources in the world. Since natural resources are limited, finding alternative energy sources becomes necessary. Biomass is abundantly available in the nature and can be an alternative to fossil fuels. Additionally, biomass is a renewable energy source. Utilizing bio-energy from biomass doesn't increase CO<sub>2</sub> emission, which is beneficial to environmental protection (Huang, Wu, Wu and Gao 2017). Bio-energy can be released through thermal chemical processes such as biomass pyrolysis, gasification, and combustion. Among them, biomass gasification is a promising technology. During the process, biomass is utilized to generate syngas, which can be further applied to generate chemicals and electricity (Ismail and El-Salam 2017).

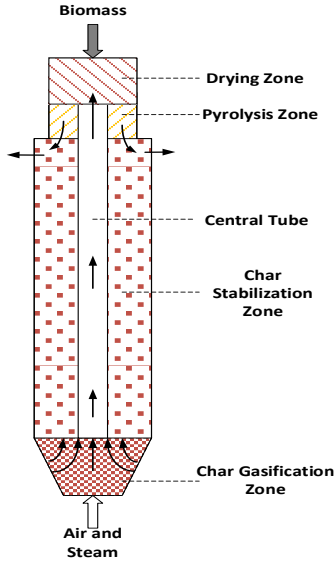


Figure 1: A circle-draft (2MWth.) biomass gasifier  
 In this work a circle-draft biomass gasifier was studied. As shown in Figure 1, biomass is fed at the top while air and steam are fed at the bottom of the gasifier. After biomass is fed to the gasifier, it is dried in the drying zone and then falls down to the pyrolysis zone where biomass is decomposed into char and volatile gases. Char particles continue to fall down and go through the stabilization zone to reach the char gasification zone where char reacts with air and steam to generate syngas. The generated syngas penetrates through the solid bed and flows upwards through a central tube to reach the upper pyrolysis zone. Biomass is heated in the pyrolysis zone while the hot syngas is flowing through the zone. Finally, the syngas is extracted through 4 outlets at the side of the gasifier.

In this work a three-dimensional CFD (computational fluid dynamics) model was developed to simulate the circle-draft biomass gasifier. In this model the MP-PIC (Multiphase Particle-In-Cell) method was applied to simulate gas-solid flows in the circle-draft biomass gasifier. The heterogeneous and homogeneous reaction kinetics were integrated with the momentum, mass, and energy transport equations to predict producer gas distribution and reactor temperature profile in the circle-draft biomass gasifier.

## MODEL DESCRIPTION

The MP-PIC method is an Eulerian-Lagrangian method. This model was built in Barracuda VR (virtual reactor). In the software, the Navier-Stokes equation was coupled with LES to simulate the gas phase. The particulate phase is calculated with the particle acceleration equation (O'Rourke and Snider 2014), based on Newton's motion law for each particle parcel. The momentum transport equation was coupled with the mass and energy transport equations to simulate mass and energy transfer in the circle-draft biomass gasifier. The calculation of thermal radiation in the MP-PIC method was based on Stefan-

Boltzmann law. The finite volume method was applied to solve the discretized governing equations.

## Governing Equations

The continuity and momentum equations for the gas phase are shown as follows:

$$\frac{\partial(\alpha_g \rho_g)}{\partial t} + \nabla \cdot (\alpha_g \rho_g u_g) = \delta m_p \quad (1)$$

$$\frac{\partial(\alpha_g \rho_g u_g)}{\partial t} + \nabla \cdot (\alpha_g \rho_g u_g u_g) = -\nabla p - F + \alpha_g \rho_g g + \nabla \cdot \tau \quad (2)$$

$$\tau = \mu \left( \frac{\partial u_{g,i}}{\partial x_j} + \frac{\partial u_{g,j}}{\partial x_i} \right) - \frac{2}{3} \mu \delta_{ij} \frac{\partial u_k}{\partial x_k} \quad (3)$$

$$\mu = \mu_{lam} + \mu_{eddy} \quad (4)$$

$\mu_{eddy}$  is calculated by the sub-grid scale (SGS) model (Smagorinsky 1963) as shown below:

$$\mu_t = \frac{1}{2} C \rho_g \Delta^2 \sqrt{\left( \frac{\partial u_{g,i}}{\partial x_j} + \frac{\partial u_{g,j}}{\partial x_i} \right)^2} \quad (5)$$

$$\Delta = \sqrt[3]{V} \quad (6)$$

$C$  is a model constant of 0.01. The particle acceleration equation is applied to calculate the particle velocity as follows (O'Rourke and Snider 2010):

$$\frac{du_p}{dt} = D_p (u_g - u_p) - \frac{\nabla p}{\rho_p} - \frac{\nabla \tau_p}{\rho_p \alpha_p} + g + \frac{\bar{u}_p - u_p}{2\tau_D} \quad (7)$$

The solid stress tensor,  $\tau_D$ , is modeled by the following equation:

$$\tau_p = \frac{10 P_s \alpha_p^\beta}{\max\{(\alpha_{cp} - \alpha_p), \varepsilon(1 - \alpha_p)\}} \quad (8)$$

$\alpha_{cp}$  is the close-pack volume fraction of the particulate phase. In this work it was set as 0.42, based on experimental data. The solid volume fraction,  $\alpha_p$ , is calculated as follows:

$$\alpha_p = \iiint f \frac{m_p}{\rho_p} dm_p du_p dT_p \quad (9)$$

The interphase momentum exchange between the gas and particle phase is given by:

$$F = \iiint f \left\{ m_p \left[ D(u_g - u_p) - \frac{\nabla p}{\rho_p} \right] + u_p \frac{dm_p}{dt} \right\} dm_p du_p dT_p \quad (10)$$

The drag function of  $D$  is described as follows (Gidaspow 1994):

$$D_{p1} = \frac{6}{8} C_d \frac{\rho_g |u_g - u_p|}{\rho_p d_p} \quad (11)$$

$$C_d = \begin{cases} \frac{24\alpha_g^{-2.65}}{Re}, Re < 0.5 \\ \frac{24\alpha_g^{-2.65}}{Re} (1 + 0.15Re^{0.687}), 0.5 \leq Re \leq 1000 \\ 0.44\alpha_g^{-2.65}, Re > 1000 \end{cases} \quad (12)$$

$$D_{p2} = 0.5 \left( \frac{180\alpha_p}{\alpha_g Re} + 2 \right) \frac{2\rho_g |u_g - u_p|}{d_p \rho_p} \quad (13)$$

$$D_p = \begin{cases} D_{p1} & \alpha_p < 0.75\alpha_{cp} \\ (D_{p2} - D_{p1}) \left( \frac{\alpha_p - 0.75\alpha_{cp}}{0.1\alpha_{cp}} \right) + D_{p1} & 0.85\alpha_{cp} \geq \alpha_p \geq 0.75\alpha_{cp} \\ D_{p2} & \alpha_p > 0.85\alpha_{cp} \end{cases} \quad (14)$$

The mass and energy transport equations for the particulate phase are (Snider, Clark and O'Rourke 2011):

$$\delta m_p = - \iiint f \frac{dm_p}{dt} dm_p du_p dT_p \quad (15)$$

$$\frac{dm_p}{dt} = \sum_{i=1}^N \frac{dm_{p,n}}{dt} \quad (16)$$

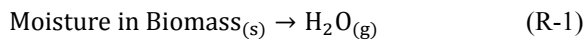
$$\frac{dm_{p,n}}{dt} = \frac{\alpha_g M_{w_{p,n}}}{\rho_p \alpha_p} m_p \frac{dc_{p,n}}{dt} \quad (17)$$

$$C_V \frac{dT_p}{dt} = \frac{1}{m_p} \frac{k_d Nu}{d_p} A_p (T_g - T_p) \quad (18)$$

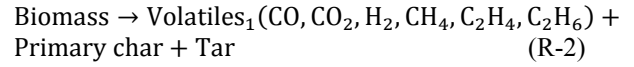
## Reaction Kinetics

In the circle-draft gasifier, biomass is fed at the top and then drops into the drying zone where moisture is released from biomass. Dry biomass continues to fall into the pyrolysis zone. Volatiles are released and char is generated from biomass pyrolysis. Char particles pass through the stabilization zone and reach gasification zone. Char particles react with air and steam injected from the bottom to generate syngas. The residual char and ash fall down into the bottom region where are removed from the gasifier with an ash auger. In this model heterogeneous reactions including biomass drying, pyrolysis, partial combustion of primary char, char and CO<sub>2</sub> reaction, char and steam reaction, and methane formation are included. The homogeneous reactions such as water gas shift reaction and gas oxidation reactions are also considered in this model.

Heterogeneous reactions (Walker Jr, Rusinko Jr and Austin 1959, Yu, et al. 2011, Xu and Qiao 2012):

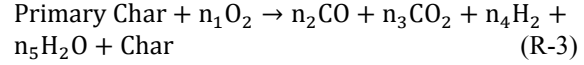


$$r_1 = 5.13 \times 10^{10} \exp\left(\frac{-10585}{T_p}\right) m_{\text{biomass}}$$



$$r_2 = 1.49 \times 10^5 \exp\left(\frac{-1340}{T_p}\right) m_{\text{biomass}}$$

The reaction rate of primary pyrolysis was calculated with a single-step global reaction mechanism (Yu, et al. 2011) and the pre-exponential factor of  $1.49 \times 10^5$  was selected to fit experimental data in this work.



$$r_3 = 8.68 \times 10^6 m_{\text{prim.char}} T_p \exp\left(\frac{-29160}{T_p}\right) [\text{O}_2]$$

The primary char generated in biomass pyrolysis was defined as CH<sub>1.286</sub>O<sub>0.4585</sub> according to experimental data. To simplify the model, char generated in the partial combustion of primary char is assumed to be pure carbon. Tar generated in biomass pyrolysis is defined as CH<sub>1.331</sub>O<sub>0.6979</sub> (Ingram, et al. 2008). The



$$r_{4f} = 1.272 m_c T_p \exp\left(\frac{-22645}{T_p}\right) [\text{CO}_2]$$

$$r_{4r} = 1.044 \times 10^{-4} m_c T_p^2 \exp\left(\frac{-2363}{T_p} - 20.92\right) [\text{CO}]^2$$



$$r_{5f} = 1.088 m_c T_p \exp\left(\frac{-22645}{T_p}\right) [\text{H}_2\text{O}]$$

$$r_{5r} = 1.044 \times 10^{-4} m_c T_p^2 \exp\left(\frac{-6319}{T_p} - 17.29\right) [\text{H}_2][\text{CO}]$$

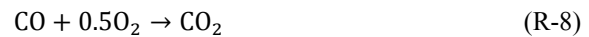


$$r_6 = 1.18 \times 10^{-5} m_c T \exp\left(\frac{-17921}{T_p}\right) [\text{H}_2]$$

Homogeneous reactions (Padban and Becher 2005, Gómez-Barea and Leckner 2010, Lu and Wang 2013):



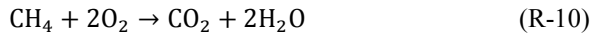
$$r_7 = 2.75 \exp\left(\frac{-10079}{T_g}\right) [\text{CO}][\text{H}_2\text{O}]$$



$$r_8 = 1.00 \times 10^{10} \exp\left(\frac{-15155}{T_g}\right) [\text{CO}][\text{O}_2]^2$$



$$r_9 = 2.2 \times 10^9 \exp\left(\frac{-13110}{T_g}\right) [\text{H}_2][\text{O}_2]^2$$



$$r_{10} = 2.8 \times 10^9 \exp\left(\frac{-24417}{T_g}\right) [\text{CH}_4][\text{O}_2]^2$$

### Simulation Setup

The CFD model was built in Barracuda Virtual Reactor<sup>®</sup> using the MP-PIC method to simulate a 2MWth circle-draft biomass gasifier at Woodland Biomass Research Center, Woodland, California, as shown in Figure 2. The height of the gasifier is 10.4 meters and the diameter of the gasifier is 1.7 meters.

The boundary settings of the circle-draft biomass gasifier are shown in Figure 3. Biomass feeding points are defined at the top, 4 gas outlets are set at the side, and steam & air injections are defined at the bottom of the gasifier.

A central tube is built in the center of the gasifier. Note that the structure of the central tube is in the shape of a rectangular box for simplicity, instead of the original cylindrical-tube shape. The total volume of the structure is still the same as that of the original central tube, which ensures that the predicted flow pattern in the gasifier is not dramatically affected by the shape change of the central tube. In the software of Barracuda VR<sup>®</sup>, geometries are meshed by orthogonal grids. For round-shaped geometries, more gridlines and cells are needed to capture necessary geometry details. In comparison, geometries with straight edges require less gridlines and computational cells. Therefore, in this work a rectangular-box channel is built to simplify the geometry to achieve better computation efficiency.

The ultimate analysis data of biomass used in experiments are shown in Table 1 and the model settings of base case are listed in Table 2. A normal distribution with a standard deviation of  $0.2d_p$  was applied to describe the size distribution of biomass particles. The thermal conductivity was set as 0.12 W/(mK) and the heat capacity of biomass was set as 1760 kJ/kgK.



Figure 2: A 2MWth circle-draft biomass gasifier

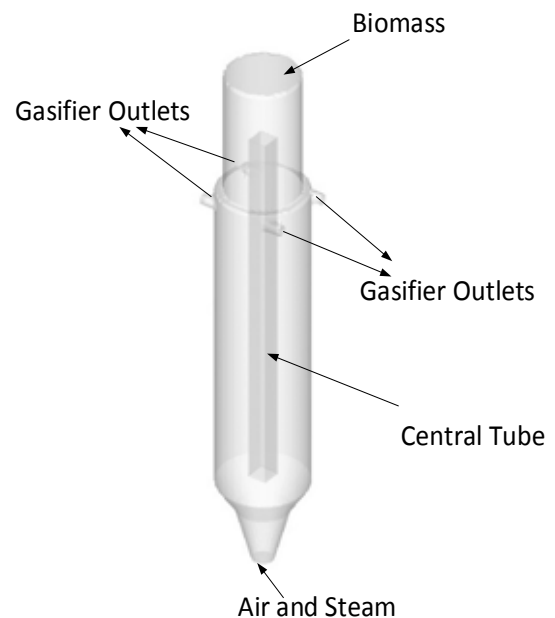


Figure 3: Boundary settings of the circle-draft gasifier

Table 1: Ultimate analysis of biomass feedstock

Elements	wt %
Moisture	17.23
C	43.16
H	5.06
O	33.26
N	0.10
Ash	1.19

Table 2: Base case settings

Description	Value
Biomass particle diameter (mm)	5.64
Biomass density (kg/m <sup>3</sup> )	662.85
Initial solid packing	0.42
Outlet pressure (atm, abs.)	1
Biomass feeding rate (kg/h)	101.42
Air feeding rate (kg/h)	77.44

The model was solved with the control volume method. A computational grid with 111,537 grid was applied for the CFD model. A grid resolution study was implemented by using three computational grids with 88,750, 111,537, and 168,175 cells. The difference of the simulation results between the three cases are less than 5%. Considering relative low computational cost and acceptable model accuracy, the grid with 111,537 cells was selected for the base case. The simulation time was set as 1000 seconds to reach the steady-state. The convergence criterions for volume, pressure, velocity, and energy were set as  $10^{-6}$ ,  $10^{-7}$ ,  $10^{-6}$ , and  $10^{-7}$ . The iteration numbers were set as 10, 2000, 50, and 100 for each transport equations, respectively. The size of time step is in the range of  $10^{-3}$  to  $10^{-5}$  seconds and is automatically controlled by the Courant-Friedrichs-Lewy (CFL) scheme (Courant, Friedrichs and Lewy 1967) to achieve a converged solution. The model was computed using the GPU-accelerated computing technology on a computer with an Intel® i7 CPU @3.50 GHz and a GeForce GTX TITAN graphics card. The 1000-s simulation took about 5 days to be completed.

## RESULTS

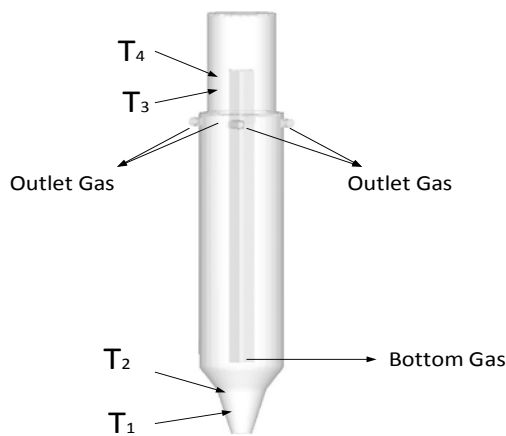


Figure 4: Temperature sensor and gas sampling locations

Figure 4 shows the locations of temperature sensors and producer gas sampling points. Considering the air and steam inlet as the bottom surface, the temperatures of  $T_1$ ,  $T_2$ ,  $T_3$ , and  $T_4$  were measured for char gasification and pyrolysis zones at the heights of 0.95, 1.44, 8.68, and 9.17 meters. Producer gas was sampled from the bottom entry point of the central tube and 4 gas outlets as the bottom

producer gas and the final producer gas output, respectively.

In Figure 5, the predicted producer gas composition in the bottom region is compared with experimental data. It is observed that the gas composition prediction in the bottom region is consistent with experiment measurement. The bottom producer gas in experiments was sampled at the bottom surface of the central tube in the circle-draft gasifier.

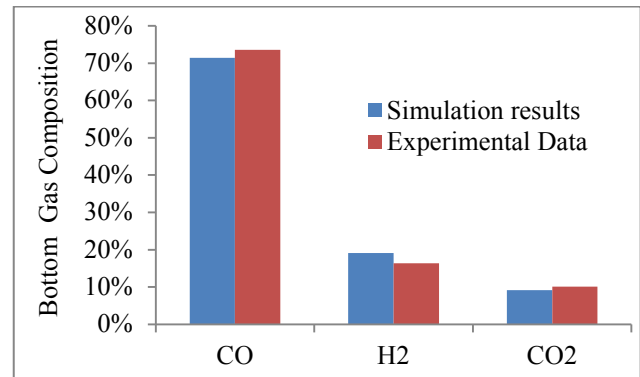


Figure 5: Comparison of bottom producer gas

The predicted outlet gas composition is also compared with experimental data. As seen in Figure 6, the difference between the simulation results and experimental data is averagely less than 3%.

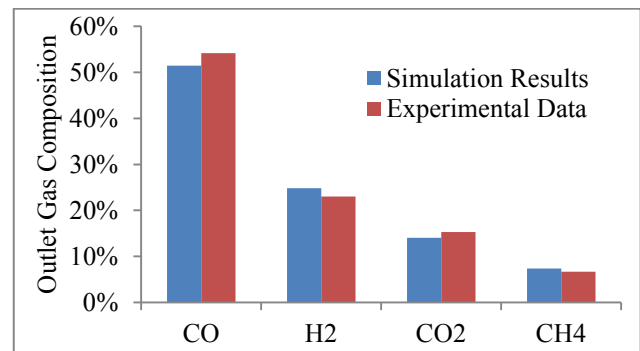


Figure 6: Comparison of outlet producer gas

Figure 7 demonstrates the comparison of the gasifier temperatures in biomass pyrolysis and char gasification zones. As seen in the figure, the temperature predictions agree well with temperature measurements.

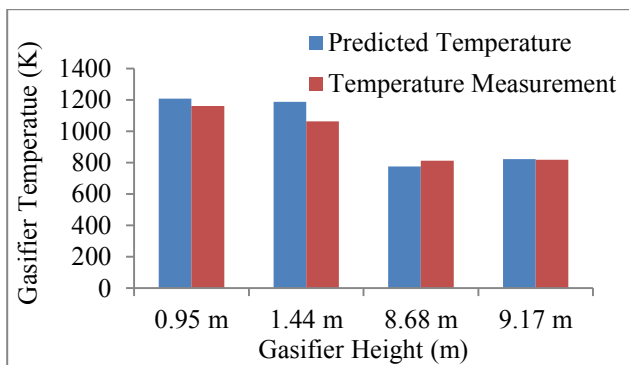


Figure 7: Comparison of gasifier temperature

Figure 8 demonstrates the transient distribution of CO molar fraction in the circle-draft gasifier. As shown in the figure, CO is generated in the bottom region due to gasification and then flows through the solid bed to reach the central tube. The gas rises through the central tube to the pyrolysis zone in the upper region of the gasifier, where more CO is generated from biomass pyrolysis. Two streams of CO from the bottom and upper regions merges and accumulates in the upper region of the gasifier. Meanwhile, the rest of CO generated in the bottom region gradually penetrates through the annular region surrounding the central tube and reaches the upper region. All of CO from the bottom and upper regions is eventually extracted from 4 gas outlets at the side of the gasifier.

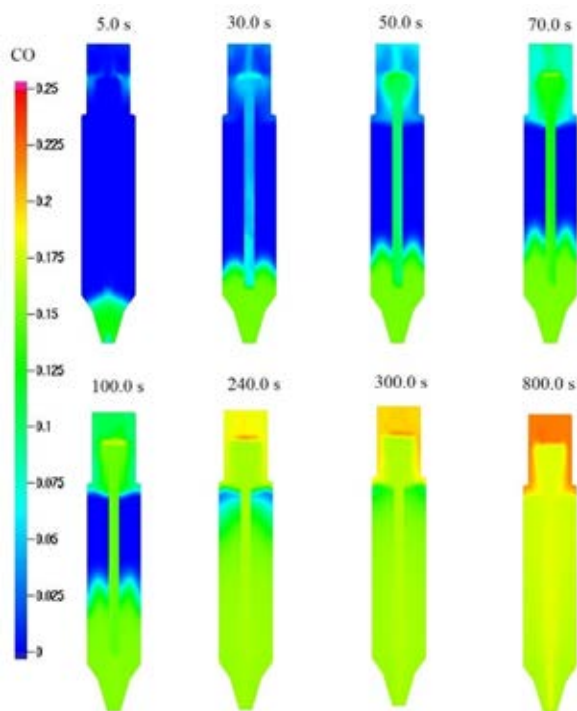


Figure 8: Transient CO distribution

Figure 9 shows transient tar distribution in the circle-draft gasifier. It is observed that tar is only generated in the pyrolysis zone which is in the upper region of the gasifier. Tar gradually accumulates in the region and finally leaves

the gasifier through the gas outlets. As predicted in the model, since tar is generated in the upper region and is extracted together with other gases from the gas outlets, tar concentration in the final gas output is expectedly high, which matches our observations in the experiment.

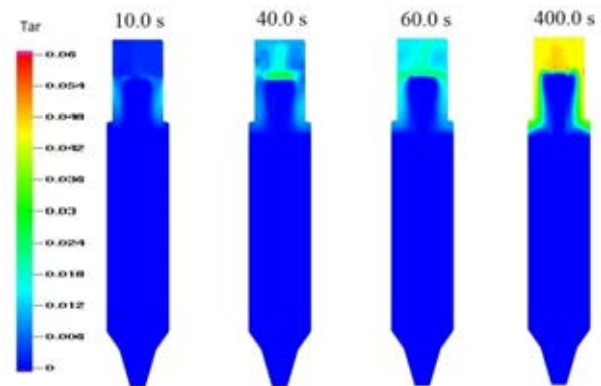


Figure 9: Transient tar distribution

The molar fractions of CO, H<sub>2</sub>, CO<sub>2</sub>, and Tar in the steady-state are shown in Figure 10. As seen in the figure, CO, H<sub>2</sub>, and CO<sub>2</sub> are generated in both of char gasification and biomass pyrolysis zones. CO and H<sub>2</sub> are concentrated in the central region, which is mainly due to producer gas production from water gas shift reaction. On the other hand, tar is only generated from the top region and is eventually extracted together with other gases through the gas outlets.

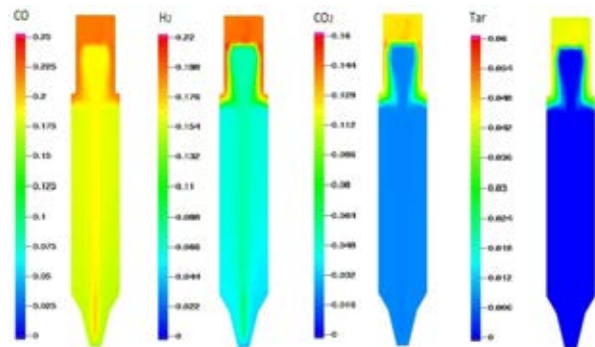


Figure 10: Steady-state producer gas composition

The temperature distribution in the circle-draft gasifier is shown in Figure 11. As indicated in the figure, the central region in the bottom region is hot due to partial combustion of char and the temperature in the upper region is lower due to biomass gasification.

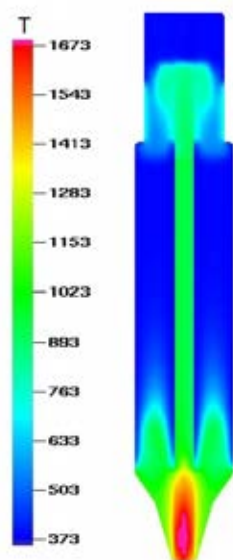


Figure 11: Temperature distribution of circle-draft biomass gasifier

## CONCLUSION

In this paper a transient three-dimensional CFD model was built to simulate a circle-draft biomass gasifier. The MP-PIC method was used to simulate gas-particle flows in the gasifier. The CFD model was applied to predict flow pattern, producer gas distribution, and reactor temperature profiles in the circle-draft biomass gasifier. The predicted gas composition and reactor temperatures were compared with experimental data and good agreement between the simulation results and experimental data was achieved.

## ACKNOWLEDGEMENT

The authors gratefully acknowledge the financial support from the California Energy Commission Grant (PIR-11-008) through West Biofuels. Additional support was provided by the University of California Discovery Pilot Research and Training Program (Award 211974).

## REFERENCES

Courant, R., Friedrichs, K., and Lewy, H. (1967), "On the Partial Difference Equations of Mathematical Physics," IBM Journal.

Gidaspow, D. (1994), "Multiphase Flow and Fluidization. Continuum and Kinetics Theory Description," Academic Press, Boston.

Gómez-Barea, A., and Leckner, B. (2010), "Modeling of Biomass Gasification in Fluidized Bed," *Progress in Energy and Combustion Science*, 36, 444-509.

Huang, S., Wu, S., Wu, Y., and Gao, J. (2017), "Structure Characteristics and Gasification Activity of Residual Carbon from Updraft Fixed-Bed Biomass Gasification

Ash," *Energy Conversion and Management*, 136, 108-118.

Ingram, L., et al. (2008), "Pyrolysis of Wood and Bark in an Auger Reactor: Physical Properties and Chemical Analysis of the Produced Bio-Oils," *Energy & Fuels*, 22, 614-625.

Ismail, T. M., and El-Salam, M. A. (2017), "Parametric Studies on Biomass Gasification Process on Updraft Gasifier High Temperature Air Gasification," *Applied Thermal Engineering*, 112, 1460-1473.

Lu, X., and Wang, T. (2013), "Water-Gas Shift Modeling in Coal Gasification in an Entrained-Flow Gasifier – Part 2: Gasification Application," *Fuel*, 108, 620-628.

O'Rourke, P. J., and Snider, D. M. (2014), "A New Blended Acceleration Model for the Particle Contact Forces Induced by an Interstitial Fluid in Dense Particle/Fluid Flows," *Powder Technology*, 256, 39-51.

O'Rourke, P. J., and Snider, D. M. (2010), "An Improved Collision Damping Time for Mp-Pic Calculations of Dense Particle Flows with Applications to Polydisperse Sedimenting Beds and Colliding Particle Jets," *Chemical Engineering Science*, 65, 6014-6028.

Padban, N., and Becher, V. (2005), "Clean Hydrogen-Rich Synthesis Gas," *CHRISGAS*, fuel from biomass.

Smagorinsky, J. (1963), "General Circulation Experiments with the Primitive Equations," *Monthly Weather Review*, 91, 99-164.

Snider, D. M., Clark, S. M., and O'Rourke, P. J. (2011), "Eulerian-Lagrangian Method for Three-Dimensional Thermal Reacting Flow with Application to Coal Gasifiers," *Chemical Engineering Science*, 66, 1285-1295.

Walker Jr, P. L., Rusinko Jr, F., and Austin, L. G. (1959), "Gas Reactions of Carbon," in *Advances in Catalysis* (Vol. Volume 11), eds. P. W. S. D.D. Eley and B. W. Paul, Academic Press, pp. 133-221.

Xu, J., and Qiao, L. (2012), "Mathematical Modeling of Coal Gasification Processes in a Well-Stirred Reactor: Effects of Devolatilization and Moisture Content," *Energy & Fuels*, 26, 5759-5768.

Yu, J., et al. (2011), "Biomass Pyrolysis in a Micro-Fluidized Bed Reactor: Characterization and Kinetics," *Chemical Engineering Journal*, 168, 839-847.